Paper n ° B2

UNSTEADY ANALYSIS OF
TRANSONIC HELICOPTER ROTOR NOISE

by

T. AOYAMA
NATIONAL AEROSPACE LABORATORY, JAPAN

K. KAWACHI
RCAST, UNIV. OF TOKYO, JAPAN

S. SAITO
NATIONAL AEROSPACE LABORATORY, JAPAN

J. KAMIO
UNIV. OF TOKYO, JAPAN

September 14-16, 1993
CERNOBBIO (Como)
ITALY

UNSTEADY ANALYSIS OF
TRANSONIC HELICOPTER ROTOR NOISE

Takashi AOYAMA
National Aerospace Laboratory
7-44-1, Jindaijihigashi-machi, Chofu, Tokyo, Japan 182

Keiji KAWACHI
Research Center for Advanced Science and Technology, the University of Tokyo
4-6-1, Komaba, Meguro-ku, Tokyo, Japan 153

Shigeru SAITO
National Aerospace Laboratory
6-13-1, Osawa, Mitaka, Tokyo, Japan 181

Jyunichi KAMIO
Department of Aeronautics, Faculty of Engineering, the University of Tokyo
4-6-1, Komaba, Meguro-ku, Tokyo, Japan 153

Abstract

A combined method of a computational fluid dynamics (CFD) technique with the extended Kirchhoff's equation has been newly developed to analyze the high-speed impulsive (HSI) noise of helicopter rotor. The method solves Euler equations by a CFD technique to obtain the pressure distributions around a rotor blade. In order to predict the HSI noise, the behavior of shock wave should be evaluated precisely. The CFD code used here has the good capability of predicting the shock wave by using a higher-order upwind scheme. In case of a forward flight condition, the Newton iterative method is used to get unsteady solutions. The Kirchhoff's equation extended for moving surfaces is then used to find the acoustic pressures by using the Euler solutions on the Kirchhoff surface in which all the acoustic sources are enclosed.

The HSI noise of a non-lifting hovering rotor is calculated by using the present method, and the good correlation between calculated and experimental results is obtained. The comparison between the HSI noise of two types of advanced tip shape and a conventional rectangular tip shape are also presented in non-lifting hovering conditions. The present method is then used to calculate the HSI noise of a non-lifting forward flight rotor. This is because the HSI noise is usually occurred in forward flight conditions.

1. Introduction

The HSI noise radiating from a transonic helicopter rotor is one of the important subjects in rotor acoustic research. In the rotor noise analysis, the method solving Ffowcs Williams and Hawkings (FW-H) equation [1] is often used. Although this method shows the good capability of predicting the noise from a subsonic rotor [2][3][4], it doesn't succeed to predict the HSI noise from a transonic rotor because it is difficult to evaluate

the quadrupole term of FW-H equation [5][6][8][9]. Another method to solve the HSI noise problem is to use a CFD technique [10] directly. This method successfully predicts the HSI noise at about three rotor radii. However, it is not practical to predict the far-field noise because of the difficulty of maintaining the adequate grid resolution in the far-field.

A combined method of CFD technique with the Kirchhoff's equation [11][12] is also used to analyze the HSI noise problem. In this method, a CFD technique is used to obtain the pressure distributions around a rotor blade. The Kirchhoff's equation is then used to find the acoustic pressures by using the CFD solutions on the Kirchhoff surface in which all the acoustic sources are enclosed. If the CFD solutions capture the nonlinear effect such as shock wave, this method can get the acoustic pressure including the effect of nonlinear sources. Previously, the full-potential equation has been used as the governing equation of CFD in spite that the behavior of shock wave should be evaluated precisely in order to predict the HSI noise. In this paper, the Euler code [13] which has the good capability of capturing the shock wave by a higher-order upwind scheme is combined with the Kirchhoff's equation extended for moving surfaces by Farassat and Myers [14].

Theoretical studies about the HSI noise has been generally conducted in hovering conditions. The HSI noise, however, usually appears in forward flight conditions. In these conditions, the key phenomenon for estimating the HSI noise, such as the delocalization and the behavior of the shock wave, become unsteady. The present method, therefore, has been developed to adapt the unsteady governing equations.

2. Calculation Method of CFD

Euler Equations

The governing equations are three-dimensional Euler equations in the blade fixed rotating Cartesian coordinate system (x, y, z) in Fig.1. In order to conduct the calculation with arbitrary curved grid, these equations are transformed from the Cartesian coordinate system to the arbitrary curvilinear coordinate system (ξ, η, ζ). The transformed equations are written as

$$\frac{\partial Q}{\partial t} + \frac{\partial F_i}{\partial \xi_i} + H = 0, \qquad (1)$$

where

$$Q = J^{-1} \begin{bmatrix} \rho \\ \rho u_1 \\ \rho u_2 \\ \rho u_3 \\ e \end{bmatrix},$$

$$F_i = J^{-1} \begin{bmatrix} \rho U_i \\ \rho u_1 U_i + \xi_{i,1} p \\ \rho u_2 U_i + \xi_{i,2} p \\ \rho u_3 U_i + \xi_{i,3} p \\ (e + p) U_i - \xi_{i,t} p \end{bmatrix},$$

$$H = J^{-1} \begin{bmatrix} 0 \\ -\rho \Omega u_2 \\ \rho \Omega u_1 \\ 0 \\ 0 \end{bmatrix}. \qquad (2)$$

In these equations,

$$
\begin{aligned}
(\ )_{,t} &= \partial/\partial t, \\
(\ )_{,j} &= \partial/\partial x_j, \\
(x_1, x_2, x_3) &= (x, y, z), \qquad (3) \\
(\xi_1, \xi_2, \xi_3) &= (\xi, \eta, \zeta), \\
(u_1, u_2, u_3) &= (u, v, w), \\
(U_1, U_2, U_3) &= (U, V, W).
\end{aligned}
$$

The quantity ρ is the density, u, v and w are the velocity components of Cartesian coordinate system, and U, V and W are components of the contravariant velocity. The quantity Ω is the angular velocity of the blade rotation, and p is the pressure which is represented as

$$p = (\gamma - 1)[e - \frac{1}{2}\rho u_i^2] \qquad (4)$$

B2-2

where γ is the ratio of specific heats and e is the total energy per unit volume. The quantity J is the Jacobian of the transformation.

Numerical Method

The numerical method to solve the governing equations is an implicit finite-difference scheme. The Euler equations are discretized in the conventional delta form using Euler backward time differencing. A diagonalized ADI method which utilizes an upwind flux-split technique is used for the implicit left-hand-side regarding the spatial differencing. In addition, a higher-order upwind scheme based on TVD is applied for the inviscid terms of the explicit right-hand-side. Each ADI operator is decomposed into the product of lower and upper bidiagonal matrices by using diagonally dominant factorization. The TVD scheme has a good capability of capturing the shock wave without adding artificial dissipations.

In order to obtain the unsteady solution in the forward flight condition of a helicopter rotor, the Newton iterative method is applied. In this method, the above-mentioned scheme

$$LHS(Q^{n+1} - Q^n) = -\Delta t RHS \qquad (5)$$

is modified as

$$LHS^m(Q^{m+1} - Q^m) =$$
$$-\Delta t(\frac{Q^m - Q^n}{\Delta t} + RHS^m) \quad (6)$$

where m means the number of the Newton iteration. In the beginning of the calculation, the steady calculation is conducted at the azimuth angle, $\psi = 90°$ by using the implicit time-marching method. Then, the unsteady calculation is started from this initial condition by using the Newton iterative method. Four iterations are sufficient to reduce the residual at each time-step. The typical dividing number along the azimuth direction is about 1000 per revolution.

For simplicity of the calculation, the algebraic method is adopted to generate the grid. The region of the grid is restricted around only one blade (see Fig.1) in order to reduce the memory and the computing time. The section of the grid has O-type shape and the grid consists of 79, 50 and 40 points for each ξ, η and ζ directions. On the blade surface, 79 and 20 points are distributed for each ξ and ζ directions and the grid is orthogonalized. The minimum grid spacing of η direction is set to 10^{-2}. A top view of the grid in the plane of rotor is shown in Fig.2. This type of swept-back grid was used by Isom et al.[11] and ensure that high grid density region followed the shock in the far-field.

All the boundary conditions are explicitly specified for simplicity. On the blade surface, non-slip and adiabatic conditions are applied. All the quantities are set to the values of free stream at the far-field and inflow boundaries. These quantities are extrapolated from the interior at the outflow boundary. The grid has cuts, and the flow properties are averaged between above and below along these cuts. In a forward flight condition, the direction of the free stream velocity observed from the blade fixed coordinate changes at every moment.

3. Calculation Method of Noise

Extended Kirchhoff's Equation

In this paper, the Kirchhoff's equation extended for moving surfaces is used to calculate the acoustic pressure. The acoustic pressure p satisfies the wave equation as follows :

$$(\frac{1}{c^2}\frac{\bar{\partial}^2 p}{\partial t^2} - \bar{\nabla}^2 p) \cdot H(f)$$
$$= -(\dot{p_n} + \frac{1}{c}M_n\dot{p_t})\delta(f) \qquad (7)$$
$$-\frac{1}{c}\frac{\bar{\partial}}{\partial t}[M_n\dot{p}\delta(f)] - \bar{\nabla}\cdot[\dot{p}n\delta(f)]$$

where $H(f)$ is the Heaviside function and $\delta(f)$ is the Dirac delta function. The quan-

tity c is the speed of sound. The Kirchhoff surface S in which all the acoustic sources are enclosed is described by $f = 0$ such that $f > 0$ defines the exterior of S. The bar over the operator symbol denotes operators involving generalized derivatives [15]. The acoustic pressure p is the function of a observer position x and a observer time t. The vector n and $M_n, \hat{p}, \hat{p}_n$ and $\hat{p}_t$ in equation (7) are described as follows :

$$n = \nabla f,$$
$$M_n = \frac{1}{c}\frac{\partial f}{\partial t},$$
$$\hat{p} = \lim_{f \to +0} p(x, t), \qquad (8)$$
$$\hat{p}_n = \nabla \hat{p} \cdot \nabla f,$$
$$\hat{p}_t = \frac{\partial \hat{p}}{\partial t}.$$

By using the Green function in unbounded space, equation (7) gives

$$p(x, t) \cdot H(f) \qquad (9)$$
$$= \int_{-\infty}^{t} d\tau \int G^0 \{-(\hat{p}_n + \frac{1}{c}M_n\hat{p}_t)\delta(f)$$
$$-\frac{1}{c}\frac{\partial}{\partial t}[M_n\hat{p}\delta(f)] - \nabla \cdot [\hat{p}n\delta(f)]\} dy,$$

where

$$G^0(y, \tau|x, t) = \frac{1}{4\pi r}\delta(g), \qquad (10)$$

and

$$g = \tau - t + \frac{r}{c}. \qquad (11)$$

In equation (9), the vector y is a source position, τ is a source time. In equation (10), r is the distance between the source and the observer positions. By performing the integration on the influential surface in equation (9), the following is obtained.

$$4\pi p(x, t) \cdot H(f)$$
$$= -\int \frac{\hat{p}_n + M_n\hat{p}_t/c}{r\Lambda}d\Sigma + \int \frac{\hat{p}\cos\theta}{r^2\Lambda}d\Sigma$$
$$+\frac{1}{c}\frac{\partial}{\partial t}\int \frac{(\cos\theta - M_n)\hat{p}}{r\Lambda}d\Sigma, \qquad (12)$$

where

$$\Lambda = \sqrt{1 + M_n^2 - 2M_n\cos\theta}. \qquad (13)$$

In equation (12), Σ is the influential surface generated by all Γ-curves as the source time τ varies from $-\infty$ to t for the fixed observer position x and time t, where the Γ-curve is the intersection of body and sphere $g = 0$. The function g is defined by equation (11) and $g = 0$ shows the sphere on which the acoustic pressure transmits in the space.

Kirchhoff Surface

The Kirchhoff surface used here is selected to correspond with the finite difference grid used in the CFD calculation. The top view of the surface is shown as the hatched region in Fig.2. The size of the surface is determined by some parametric studies. The station of its outer base in x axis is about 1.1 rotor radii and the line of apsides of the every section is about 4 blade chords. In the calculation of a forward flight, since the pressure distributions on the Kirchhoff surface vary at every azimuth position, they are previously calculated by using unsteady Euler solutions at 20 azimuth position clustered around advancing side and they are interpolated at any azimuth positions.

4. Results and Discussions

HSI noise in Hover

At the first step of this research, the HSI noise in hover is calculated by the present method. Fig.3 shows the calculated and experimental [4] acoustic pressures of a 1/7-scale model of a UH-1H main rotor in hover. The model rotor has a NACA 0012 airfoil section and the aspect ratio is 13.71. The calculations are made for two cases. One is the condition of tip Mach number is 0.88 [case(a)] and the other is that of tip Mach number is 0.90 [case(b)]. The quantity M_T is tip Mach number, μ is advance ratio and r/D is the distance between the observer position and the center of the rotor nondimensionalized by the blade diameter. In comparison between the results

of the present method and of the FW-H equation without quadrupole term, it becomes clear that the quadrupole sources play an important part in prediction of the HSI noise. The results of the present method also predict the experimental data better than those of the FW-H equation including the quadrupole term [6] particularly in case(b).

Fig.4 shows the Mach contours around a blade tip in the two cases. The Mach contours of case(b) indicates the occurrence of the delocalization phenomena.

HSI Noise of Advanced Tip Shape

Fig.5 shows the comparisons of acoustic pressure of an advanced tip shape similar to BERP [7] with a rectangular tip shape. The airfoil section is NACA0012 at every radial station for both shapes in order to make clear the planform effect alone on the acoustic pressure. It should be notified that the advanced tip shape is thicker than the rectangular tip shape. The calculations are made for two cases mentioned above. In case(a), the negative peak pressures of both the blade tips are nearly equal to each other as shown in Fig.5(a). The delocalization is not observed for either tip shape as shown in Figs.4(a) and 6(a). In addition, the shock wave on the rectangular tip shape is a little stronger than that on the advanced tip shape. Therefore, it is estimated that the shock wave effect on the acoustic pressure is almost canceled by the thickness effect. In contrast, the absolute value of the negative peak pressure of the advanced tip shape in case(b) is much less than that of the rectangular tip shape, as shown in Fig.5(b). This is because the delocalization for the advanced tip shape is disappeared as shown in Fig.6(b) and because the strength of the shock wave of the advanced tip shape is much less than that of the rectangular tip shape.

Fig.7 shows the comparisons of acoustic pressure between a rectangular tip shape and an advanced tip shape similar to ONERA PF2 [16]. In case(a), the absolute value of the negative peak pressure of the advanced tip shape is much less than that of the rectangular tip shape because the blade thickness decreases and the shock wave on the blade surface weakens as shown in Figs.4(a) and 8(a). In case(b), although the delocalization slightly occurs, the absolute value of the negative peak pressure of the advanced tip shape is less than that of the rectangular tip shape because the shock wave on the blade surface weakens as shown in Figs.4(b) and 8(b).

Results of CFD in Forward Flight

Before the calculation of the HSI noise in forward flight, the validation of the CFD results by using the swept-back grid in Fig.2 is conducted. Fig.9 shows the comparisons between the calculated and experimental pressure distributions of a model rotor in forward flight. The experimental data was obtained at the Army Aeroflightdynamics Directorate (AFDD) [17]. The model rotor has a NACA 0012 airfoil section and the aspect ratio is 7.125. The quantity M_T is tip Mach number, μ is advance ratio, x/C is the chordwise distance nondimensionalized by chord length and r/R is the radial station nondimensionalized by the blade radius. It is indicated that the calculated results are in good agreement with the experimental data in every azimuth position for these two radial stations. Therefore, the capability of the present calculation method is verified.

HSI noise in Forward Flight

The HSI noise in non-lifting forward flight is calculated for the following :
case(1) : $M_T = 0.666$, $M_{AT} = 0.864$
case(2) : $M_T = 0.666$, $M_{AT} = 0.896$
case(3) : $M_T = 0.666$, $M_{AT} = 0.916$
where M_{AT} is advancing tip Mach number. Figs.10 and 11 show the calculated result of the variation of the acoustic pres-

sure for the increase of the advancing tip Mach number, and Fig.12 shows the Mach contours around a blade tip. The delocalization doesn't occur at the advancing side in cases (1) and (2), but it occurs from about $\psi = 80°$ to $110°$ in case (3), where ψ is azimuth angle. It is estimated from these figures that the absolute value of the negative peak pressure grows rapidly when the delocalization occurs.

5. Conclusions

- A combined method of a CFD technique with the extended Kirchhoff's equation has been developed to analyze the HSI noise of helicopter rotor.

- The acoustic pressure of a model helicopter rotor is predicted well by the present method in non-lifting hovering conditions.

- The acoustic pressures for the advanced tip shapes similar to BERP and ONERA PF2 on the HSI noise in non-lifting hover are presented.

- It is indicated that the CFD results by using the swept-back grid are in good agreement with the experimental data for the pressure distributions on a blade surface in forward flight.

- The calculated results of the HSI noise in non-lifting forward flight is also presented by using the present method.

References

1. J.E.Ffowcs Williams and D.L.Hawkings, Sound Generation by Turbulence and Surface in Arbitrary Motion, Philosophical Trans. of the Royal Society of London, Series A, vol.264, 321-342, 1969.

2. F.Farassat, Theory of Noise Generation from Moving Bodies with an Application to Helicopter Rotors, NASA TR R-451, 1975.

3. Y.Nakamura and A.Azuma, Rotational Noise of Helicopter Rotors, Vertica, vol.3, no.3/4, 293-316, 1979.

4. D.A.Boxwell, Y.H.Yu and F.H.Schmitz, Hovering Impulsive Noise : Some Measured and Calculated Results, Vertica Vol.3, 1979.

5. D.B.Hanson and M.R.Fink, The Importance of Quadrupole Sources in Prediction of Transonic Tip Speed Propeller Noise, Journal of Sound and Vibration, vol.62, no.1, 1979.

6. F.H.Schmitz and Y.H.Yu, Transonic Rotor Noise - Theoretical and Experimental Comparisons, Vertica vol.5, no.2, 1981.

7. Private Letter from Kawasaki Heavy Industry.

8. H.R.Aggarwal, The Calculation of Transonic Rotor Noise, AIAA Journal, vol.22, no.7, 1984.

9. J.Prieur, Calculation of Transonic Rotor Noise Using Frequency Domain Formulation, AIAA Journal, vol.26, no.2, 1988.

10. J.D.Baeder, Euler Solutions to Nonlinear Acoustics of Non-lifting Hovering Rotor Blades, 16th European Rotorcraft Forum, 1990.

11. M.Isom, T.W.Purcell and R.C.Strawn, Geometrical Acoustics and Transonic Helicopter Sound, AIAA paper 87-2748, 1987.

12. T.W.Purcell, A Prediction of High Speed Rotor Noise, AIAA paper 89-1132, 1989.

13. T.Aoyama, K.Kawachi and S.Saito, Unsteady Calculation for Flowfield of Helicopter Rotor with Various Tip Shape, 18th European Rotorcraft Forum, 1992.

14. F.Farassat and M.K.Myers, Extension of Kirchhoff's Formula to Radiation from Moving Surfaces, Journal of Sound and Vibration, vol.123, no.3, 1988.

15. F.Farassat, Discontinuities in Aerodynamics and Aeroacoustics : the Concept and Applications of Generalized Derivatives, Journal of Sound and Vibration, vol.55, no.2, 1977.

16. J.J.Philippe and J.J.Chattot, Experimental and Theoretical Studies on Helicopter Blade Tips at ONERA, ONERA TP 1980-96, 1980.

17. J.O.Bridgeman, R.C.Strawn and F.X.Caradonna, An Entropy and Viscosity Corrected Potential Method for Rotor Performance Prediction, 44th Annual Forum of the American Helicopter Society, 1988.
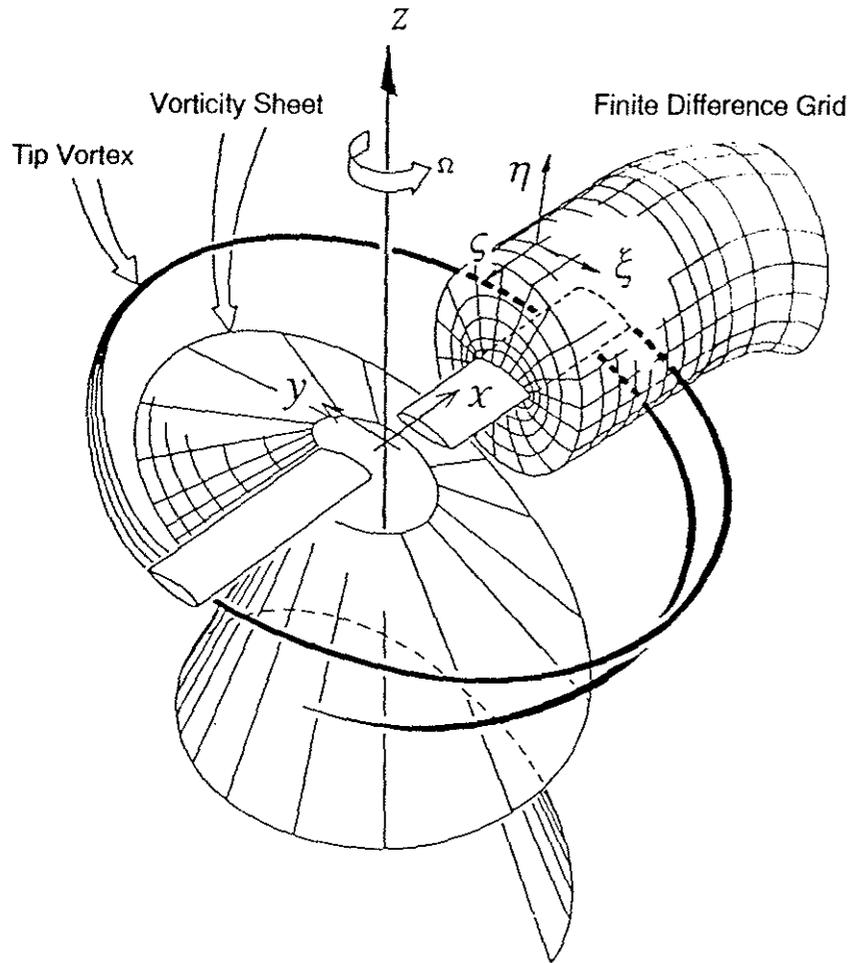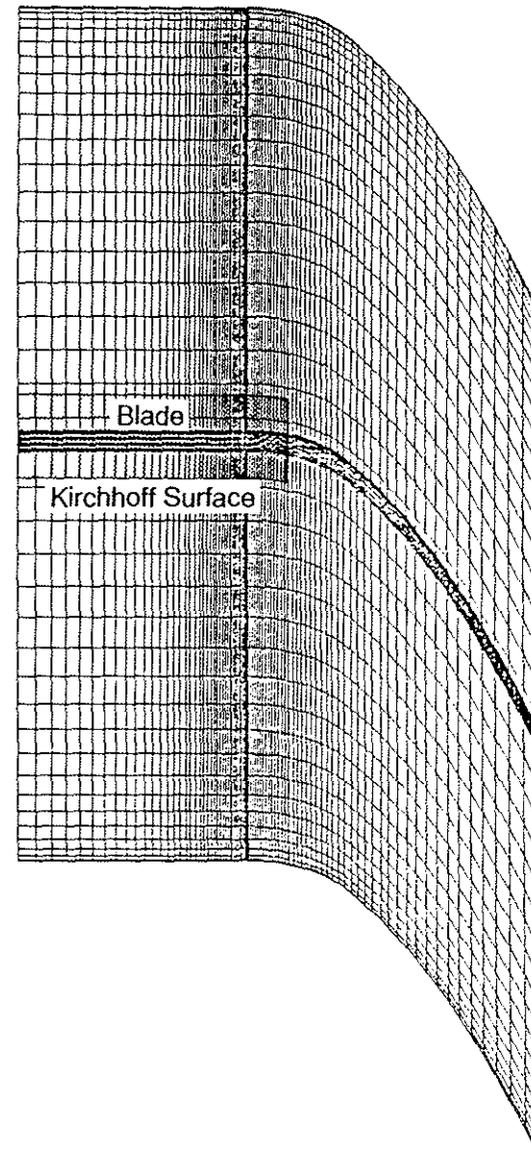
Fig.1 Coordinate system and grid.
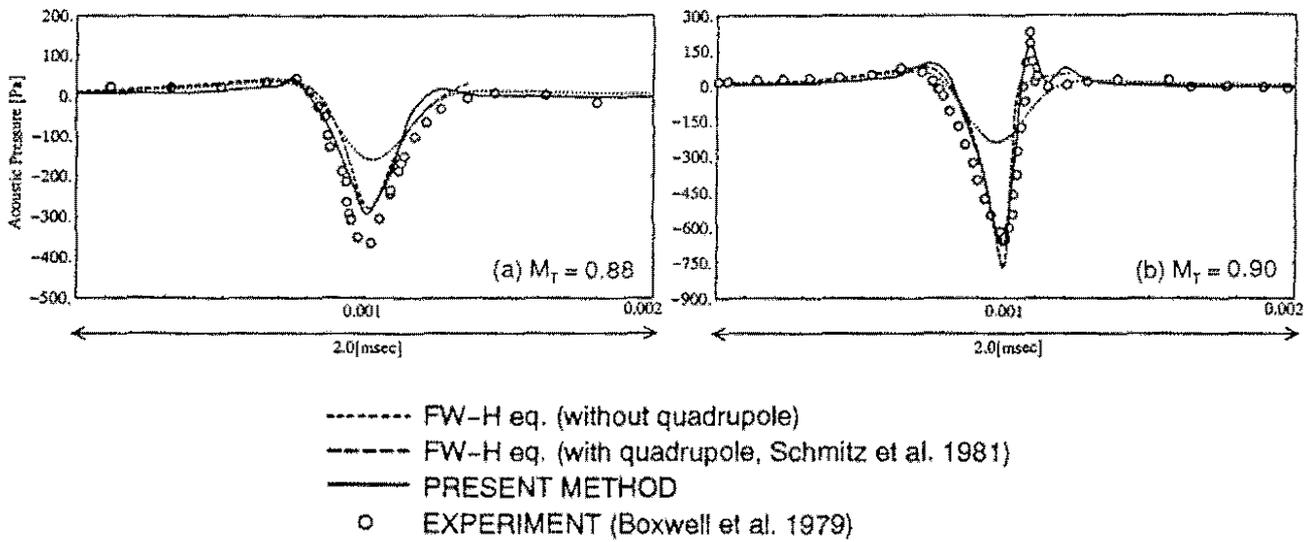

Fig.2 Top view of the grid.

----- FW–H eq. (without quadrupole)
------ FW–H eq. (with quadrupole, Schmitz et al. 1981)
——— PRESENT METHOD
○ EXPERIMENT (Boxwell et al. 1979)

Fig.3 Acoustic pressure in non–lifting hover condition ;
blade shape (AR=13.71, NACA0012), source position (in–plane, r/D=1.5).

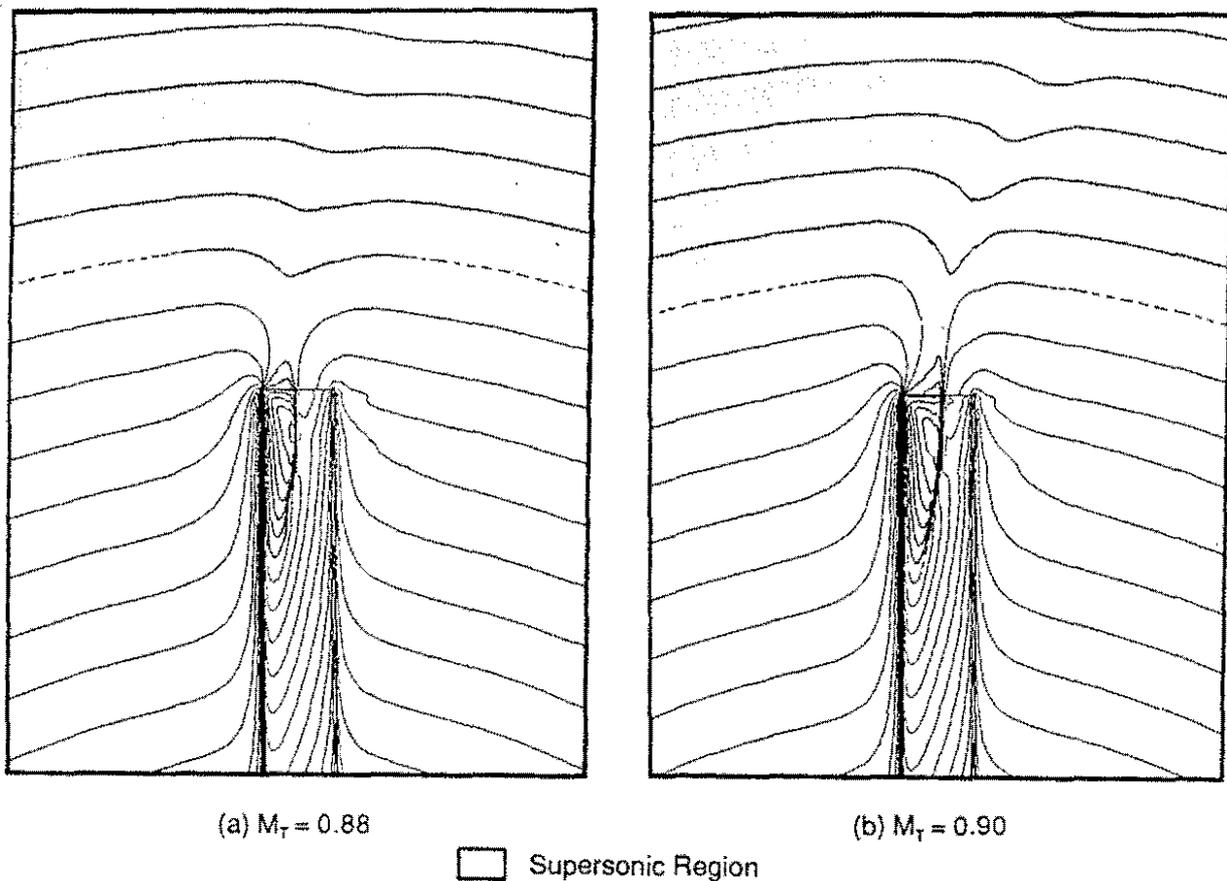(a) M_T = 0.88   (b) M_T = 0.90

☐ Supersonic Region

Fig.4 Mach contour around a blade tip.
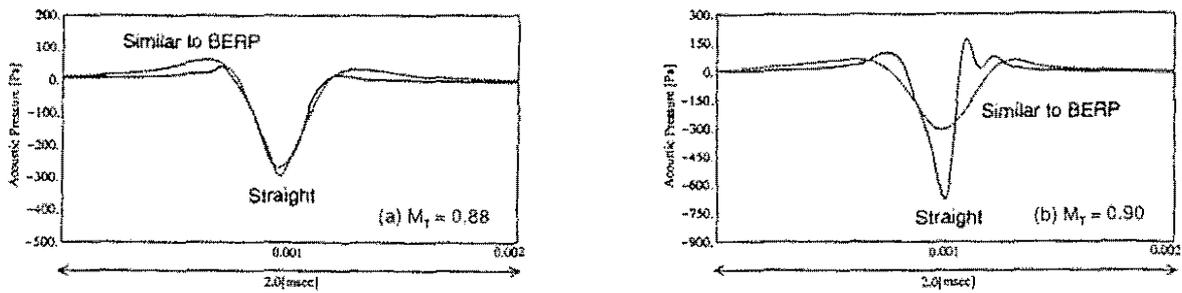
Fig.5 Comparison of acoustic pressure between rectangular tip shape and advanced tip shape similar to BERP ; blade shape (AR=13.71, NACA0012), source position (in-plane, r/D=1.5).
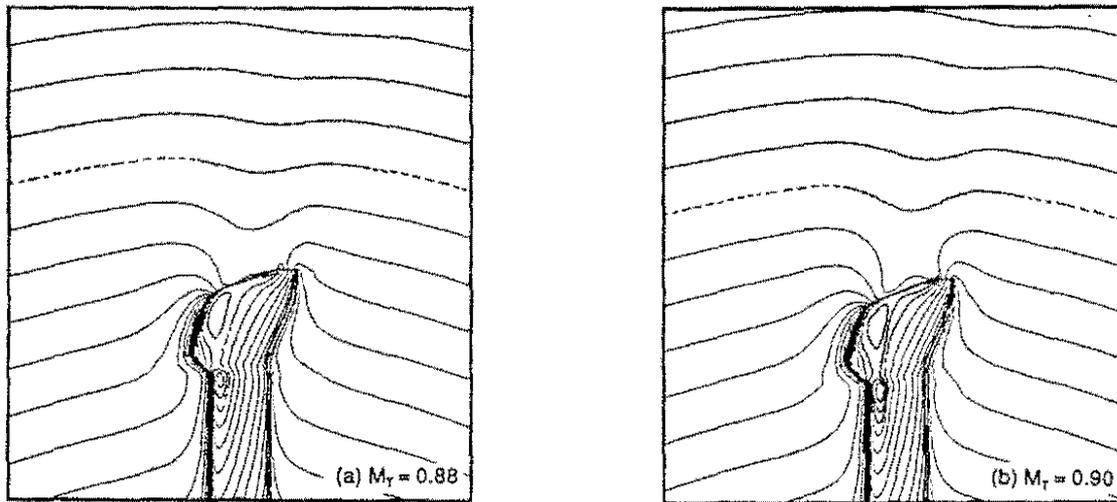
Fig.6 Mach contour around a blade (Advanced tip shape similar to BERP). ☐ Supersonic Region
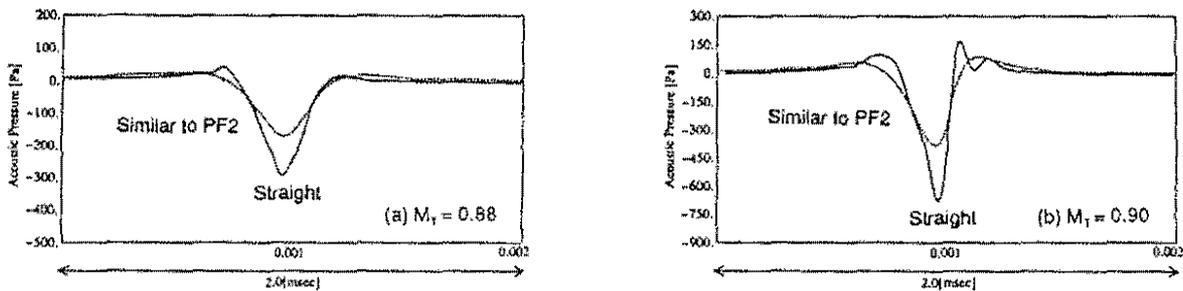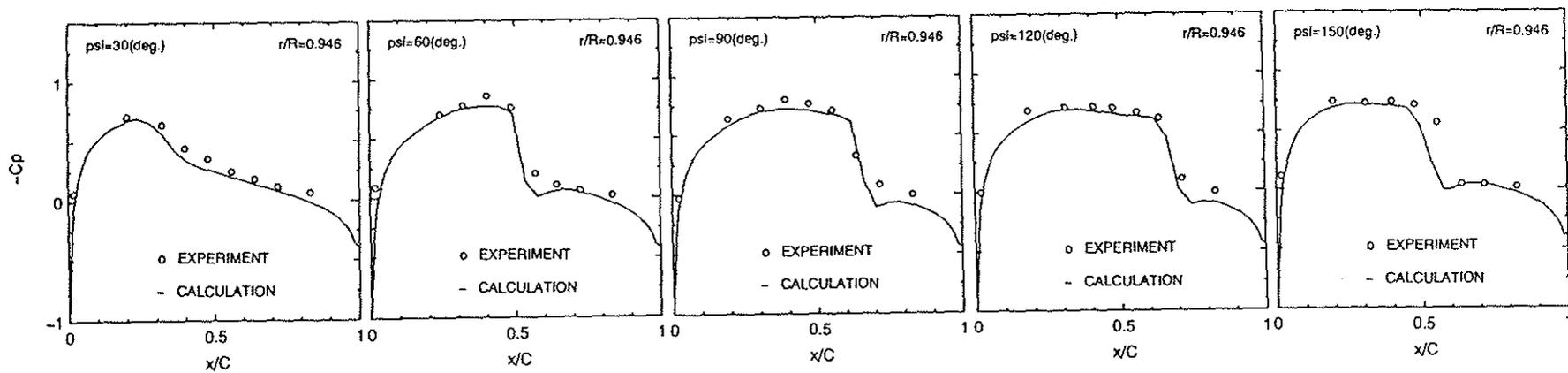

Fig.7 Comparison of acoustic pressure between rectangular tip shape and advanced tip shape similar to PF2 ; blade shape (AR=13.71, NACA0012), source position (in-plane, r/D=1.5).
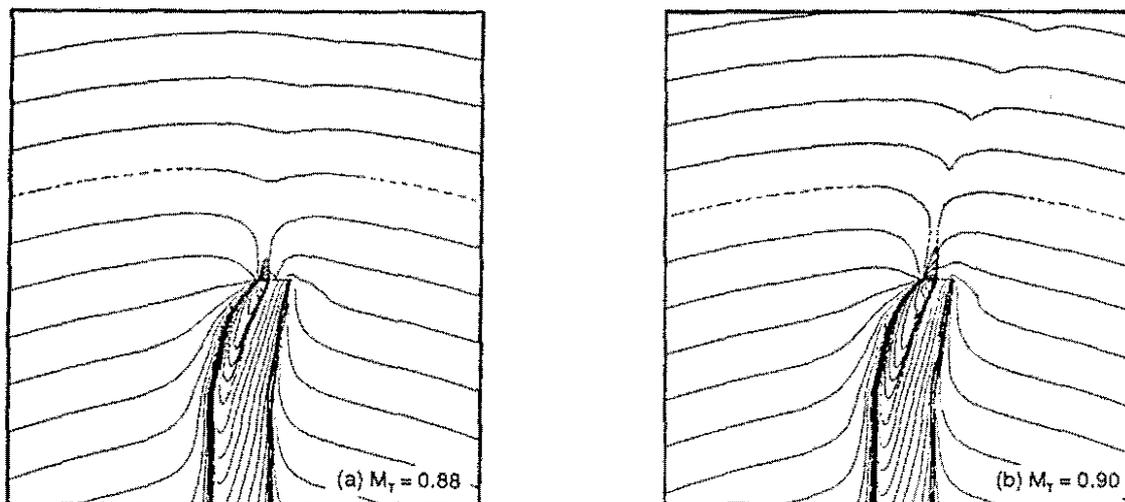
Fig.8 Mach contour around a blade (Advanced tip shape similar to PF2). ☐ Supersonic Region

B2-9
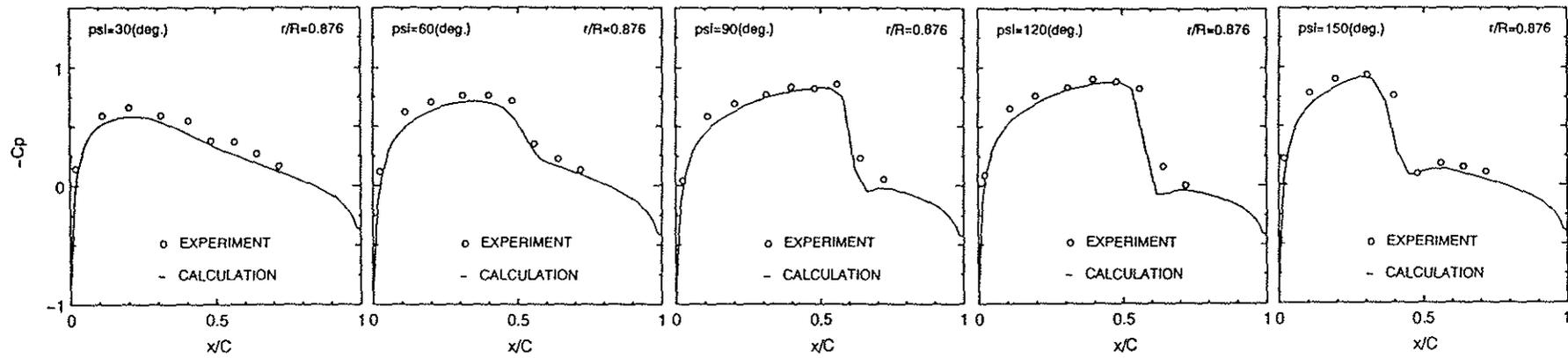
(a) $M_T = 0.763$, $\mu = 0.246$, $r/R = 0.876$

(b) $M_T = 0.763$, $\mu = 0.246$, $r/R = 0.946$

Fig.9 Surface pressure distribution in non–lifting forward flight ;
AR=7.125, NACA0012.
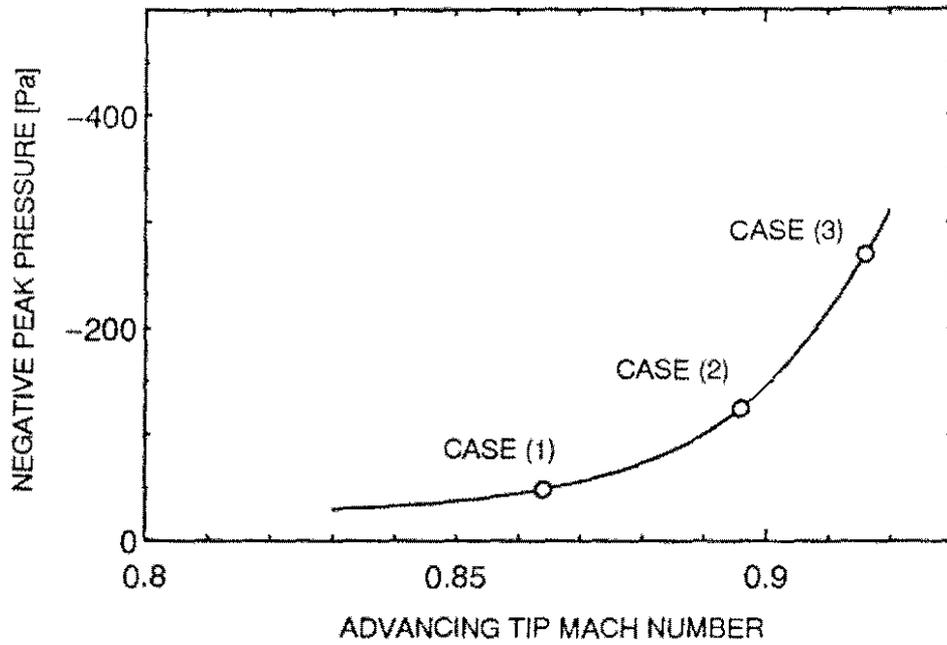
Fig.10 Negative peak pressure vs tip Mach number in forward flight ; blade shape
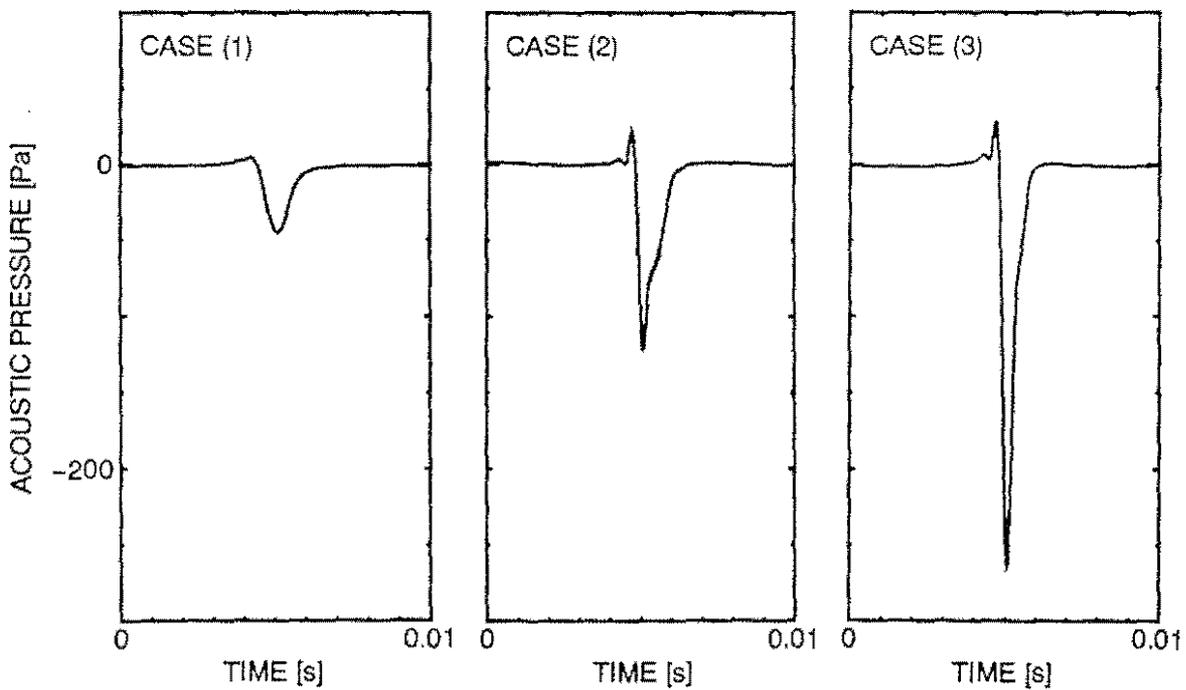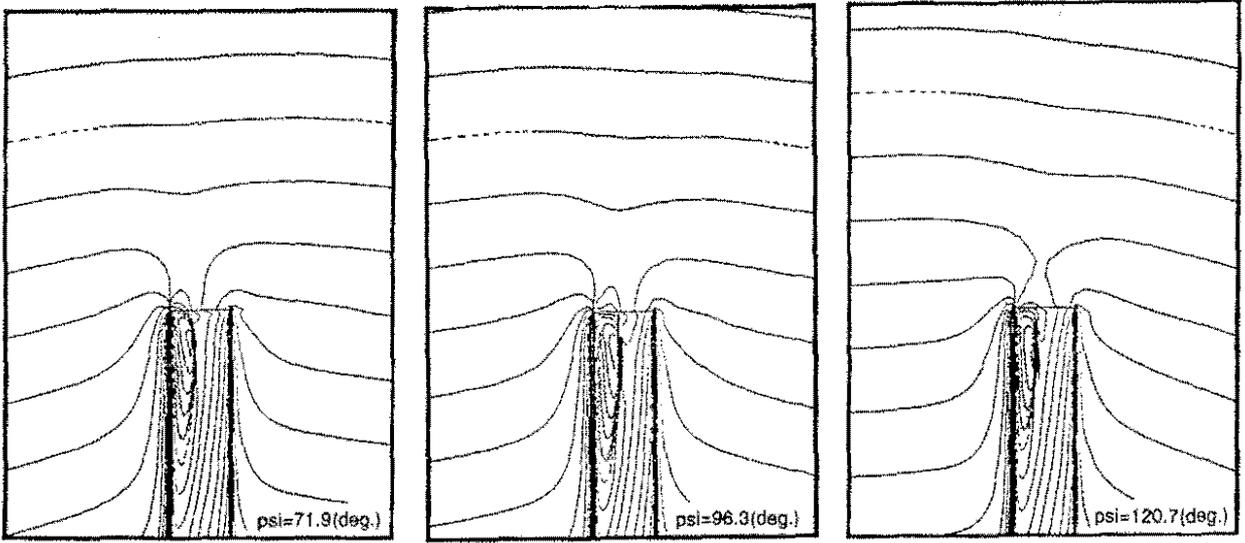(AR=13.71, NACA0012), source position (in–plane, r/D=1.5, psi=180(deg.)).

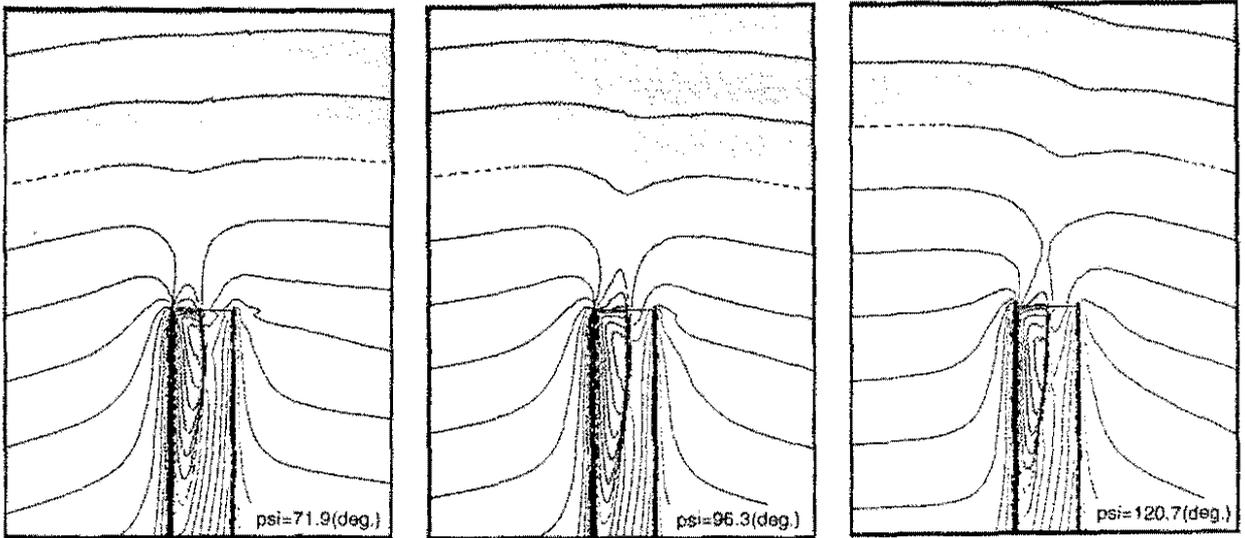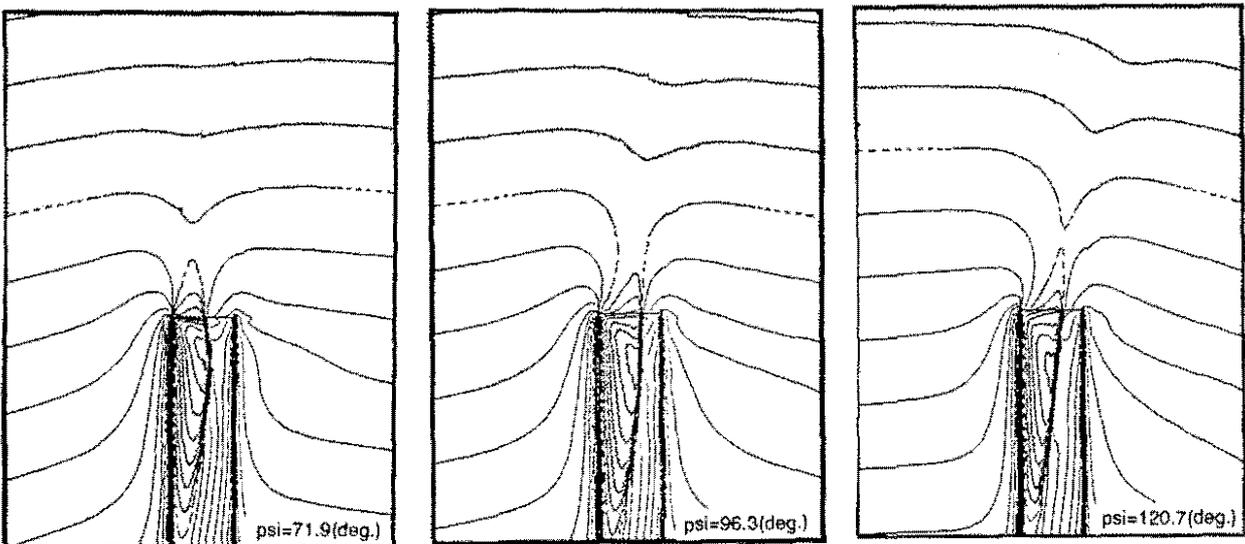Fig.11 Time history of acoustic pressure.

Fig.12 Mach contour around a blade tip in forward flight. ☐ Supersonic Region